Materials and Methods

Instrumentation

(a) Hitachi TM1000 SEM: For the image presented in Fig. 1A the spicules were deposited on a silicon wafer, not coated, and were imaged in the back-scattered electron (BSE) imaging mode, at a fixed voltage of 15 kV, at the Electron Microscopy Laboratory, University of California - Berkeley.

(b) Zeiss Ultra-Plus FEG-SEM: A Schottky field emission gun scanning electron microscope (FEG-SEM), with magnification ×12 to ×1,500,000; accelerating voltage, 200 V− 30 kV, and probe current 4 pA− 20 nA.

(c) FEI Tecnai G2 T20 S-Twin 200 keV (or 120 keV) TEM with a LaB6 electron source and a FEI Supertwin Objective Lens.

(d) FEI Titan 80-300 keV S/TEM, which includes corrector and monochromator technologies enabling resolution of 0.7 Å.

(e) FEI Strata 400S Dual-Beam system, a fully digital FEG-SEM equipped with FIB technology and a Flipstage-STEM assembly. It provides for complete in-situ sample preparation and high-resolution analysis.

(f) High-resolution X-ray powder diffraction measurements were carried out at the dedicated Beamline ID31 of the European Synchrotron Radiation Facility (ESRF, Grenoble, France), which is equipped with a crystal-monochromator and crystal-analyzer optical elements of the incident and diffracted beams, respectively. X-rays from the synchrotron storage ring were monochromatized by a liquid-nitrogen-cooled double-crystal silicon monochromator. The optics of the diffracted beam consisted of nine (111)Si crystal-analyzers. Use of the advanced analyzing optics yielded diffraction spectra of superior quality and, of particular importance, intense and extremely narrow diffraction peaks whose contribution to the peak widths did not exceed 0.004° (Fitch, 2004 (*28*)). Calibration of the instrument and wavelength refinement were performed with standard silicon samples from the National Bureau of Standards and Technology (NIST, Gaithersburg, MD, USA). Powders were loaded into borosilicate glass capillaries of diameter 0.5–1 mm. Intensity spikes from individual crystallites subjected to quasi-parallel synchrotron beam irradiation were avoided by rotation of the samples at 60 rps during measurements.

Sample preparation and characterization

(a) *Preparation of a batch of Herdmania momus vateritic spicules*

Herdmania momus specimens for this study were collected by scuba diving from marine floats in Eilat at the northern tip of the Gulf of Aqaba (Red Sea), Israel. Specimens were cut into small tissue pieces, which were then treated with 7% sodium hypochlorite (NaOCl) to remove the organic matter. NaOCl was replaced frequently and vials were shaken gently for 6 weeks until all organic matter was removed. Spicules were filtered to remove debris and washed 3 times in 100% ethanol.

(b) *SEM sample preparation*. Spicules were placed on an aluminum SEM sample holder directly from storage in pure ethanol. Samples were air-dried and then coated with nanometer-thick amorphous carbon.

(c) *TEM sample preparation*. Spicules were prepared as for the SEM samples. After they were mounted and coated, FIB was utilized to prepare thin lamellae (in different

directions). Preparation of lamellae involved several steps: first, the region of interest on the spicule was coated with up to 3 μm of platinum by the use of both electron-beam deposition and ion-beam deposition within the FIB vacuum chamber. Next, each lamella was further cut and thinned so that TEM specimens could be lifted off the sample holder. During the lifting process each lamella was transferred to a molybdenum TEM grid for further thinning with a gallium ion beam.

(d) *Samples for synchrotron radiation diffraction*. For powder diffraction, biogenic vaterite spicules were gently ground with a mortar and pestle. The measured X-ray powder diffraction profiles were subjected to Rietveld refinement within the GSAS program (Larson and Von Dreele, 2004) (*29*) and the EXPGUI interface (Toby, 2002 (*30*)). Using the Rietveld method we tried to fit the experimental X-ray diffraction spectrum to each of the proposed crystal structures of vaterite. As described in the manuscript, the Kamhi model gave the best fit with a goodness of fit of chi-square around 14 (see Fig. S1). The orthorhombic structure proposed by Meyer gave chi-square of 16. The other models gave chi-square values of above 100, which showed that they did not fit.

TEM electron diffraction and imaging

To verify the results and conclusions, we used a variety of methods to solve the electron diffractions. Figure S2 shows, as an example, how an electron diffraction was solved using the JEMS Electron Microscopy Software Package (Version 3.1102W2006, Copyright: P. Stadelmann, 1999–2006), a program for the simulation of electron diffraction patterns and high-resolution images). The Kamhi and Meyer models are in the same zone axis. In this zone axis, it can be clearly seen that neither the Kamhi nor the Meyer model could explain the entire diffraction pattern. Other structural models gave different partial solutions or no solution at all.

Using a zone axis proposed by the diffraction image solution within the framework of a specific structural model, we performed atomic simulation to examine whether the phase-contrast image also yielded a good fit. The atomic simulations were performed using the DIMA program (a software developed by Dr. Yaron Kauffman of the Department of Materials Science and Engineering at the Technion, Haifa). Table S1 presents an example showing how the fitting percentage was obtained.

Figure S4 shows that the planar defects are not a result of the sample preparation (FIB) because the same defects can be observed with a different method of preparation, namely by etching via Ar ion bombardment.

Ruling out radiation damage artifacts

Along the [001] zone axis we see a rotation of 30° between the main and minor structures, and the relation $a' = \sqrt{3}\,a$ is identical to that found by Kamhi (and erroneously attributed to a supercell), who used lab-source X-Ray Diffractometry (XRD) and not e-beam in TEM. Hence the minor structure could not have been due to beam damage.

Furthermore, the rotation by exactly 30° and the $a' = \sqrt{3}\,a$, is a relationship which cannot occur by chance. Electron beam damage would produce an arbitrary array of random modifications, not rotations or a distinct structure.

Supplementary Text

Additional information on the intracrystalline organic phase in thorns of the vateritic spicule

Use of the FIB to prepare a sample from a single thorn enabled us to observe a zone axis parallel to [001]. Figure S4A,B shows the bright contrast circles, implying a lower atomic number than that of the calcium phase, and instead representing the organic phase.

FFT from phase-contrast images

It is vital to show that the minor structure is not merely one of the other two anhydrous calcium carbonate polymorphs (calcite or aragonite). Table S2 provides a summary of the d-spacing attained from the FFT in Fig. 4F and the d-spacing in the range for calcite and aragonite.

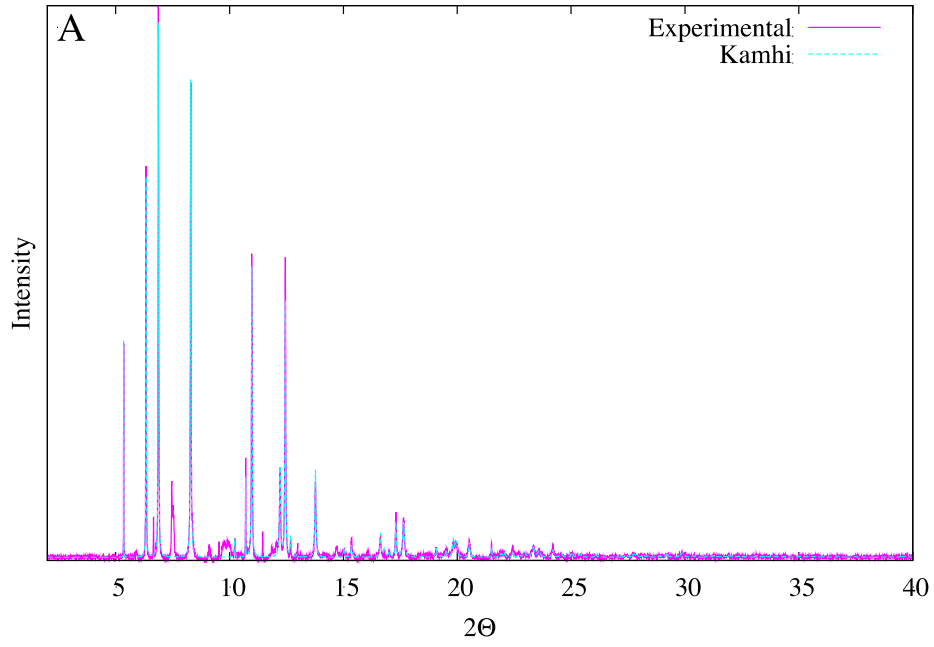
A
Experimental
Kamhi
Intensity
5
10
15
20
25
30
35
40
2Θ

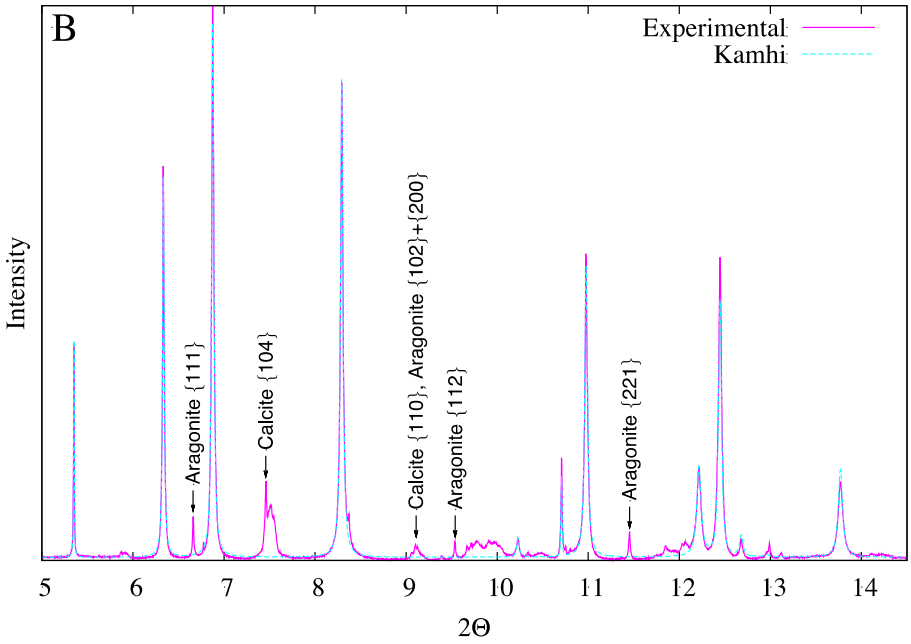
B
Experimental
Kamhi
Intensity
Aragonite {111}
Calcite {104}
Calcite {110}, Aragonite {102}+{200}
Aragonite {112}
Aragonite {221}
5
6
7
8
9
10
11
12
13
14
2Θ

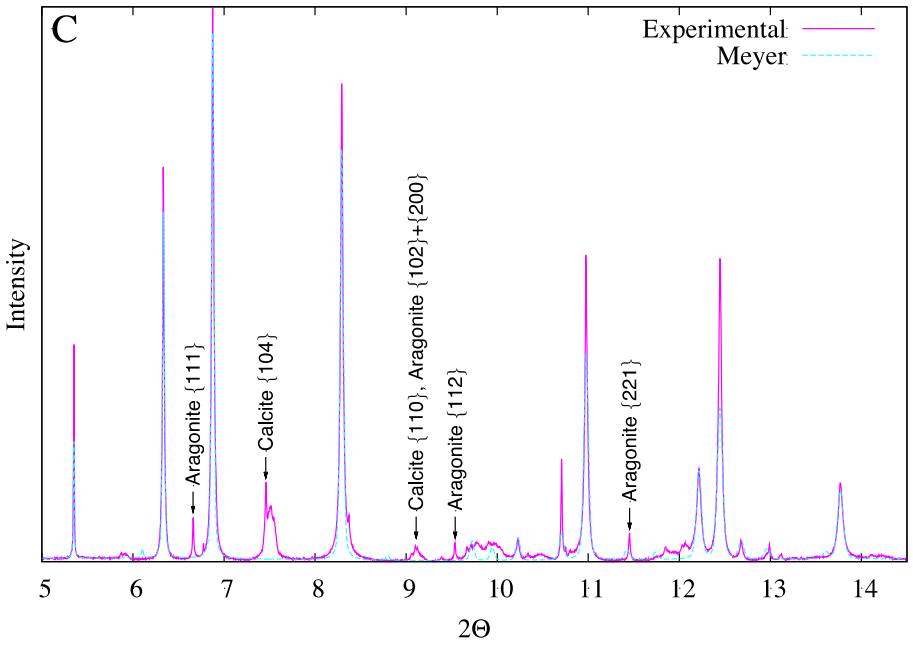
C
Experimental
Meyer
Intensity
Aragonite {111}
Calcite {104}
Calcite {110}, Aragonite {102}+{200}
Aragonite {112}
Aragonite {221}
5
6
7
8
9
10
11
12
13
14
2Θ

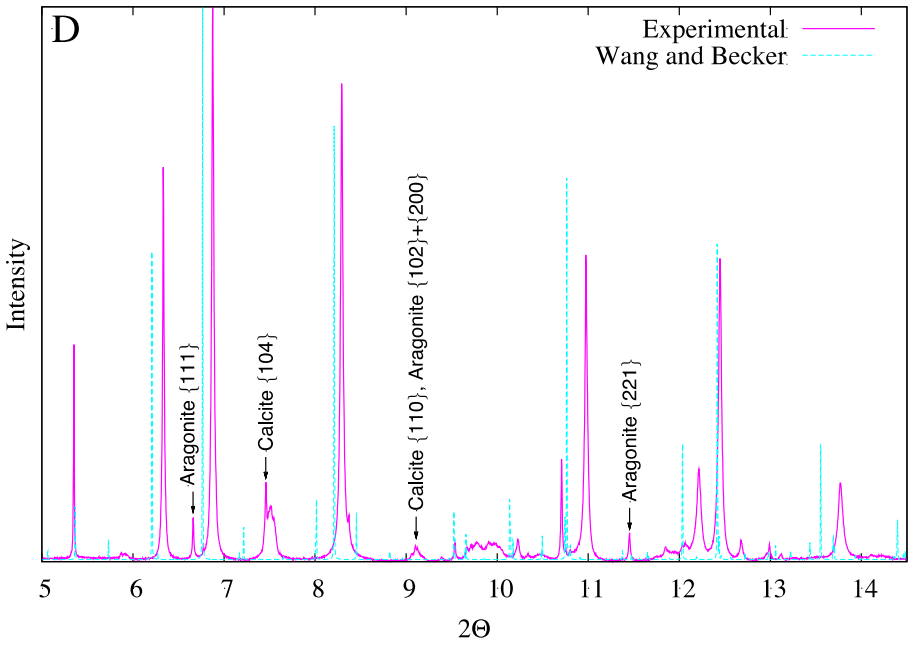
D
Experimental
Wang and Becker
Intensity
Aragonite {111}
Calcite {104}
Calcite {110}, Aragonite {102}+{200}
Aragonite {221}
5
6
7
8
9
10
11
12
13
14
2Θ

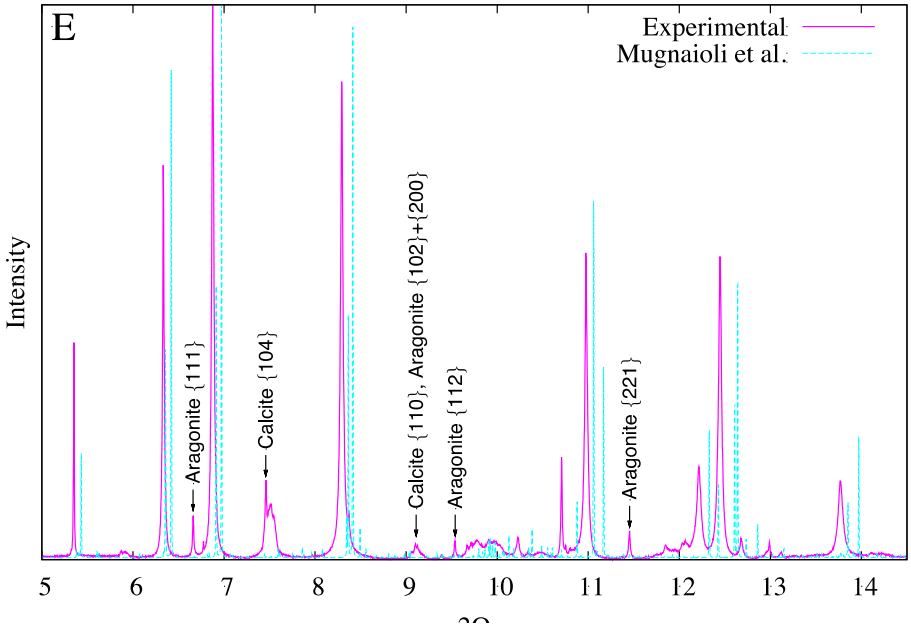

Fig. S1

High-resolution X-ray powder diffraction spectra. (A) Biogenic vaterite entire spectrum and the calculated Kamhi model spectrum. (B– E) Biogenic vaterite spectra in selective angular range between 5° to 14.5° and the calculated spectrum of (B) Kamhi model. (C) Meyer Orthorhombic model. (D) Wang and Becker model (E) and the Mugnaioli triclinic model. All diffraction spectra were obtained at wavelength (λ) = 0.394796 Å.

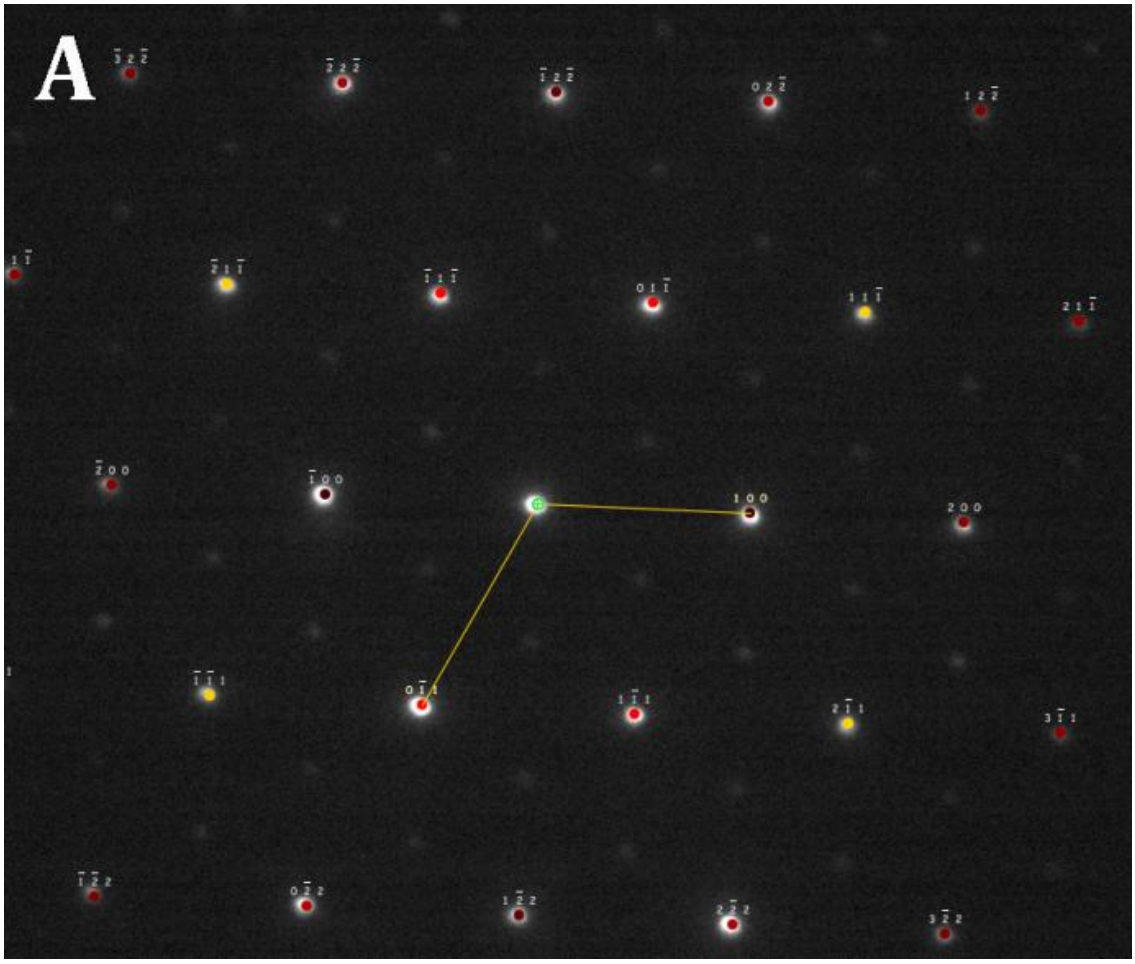
A

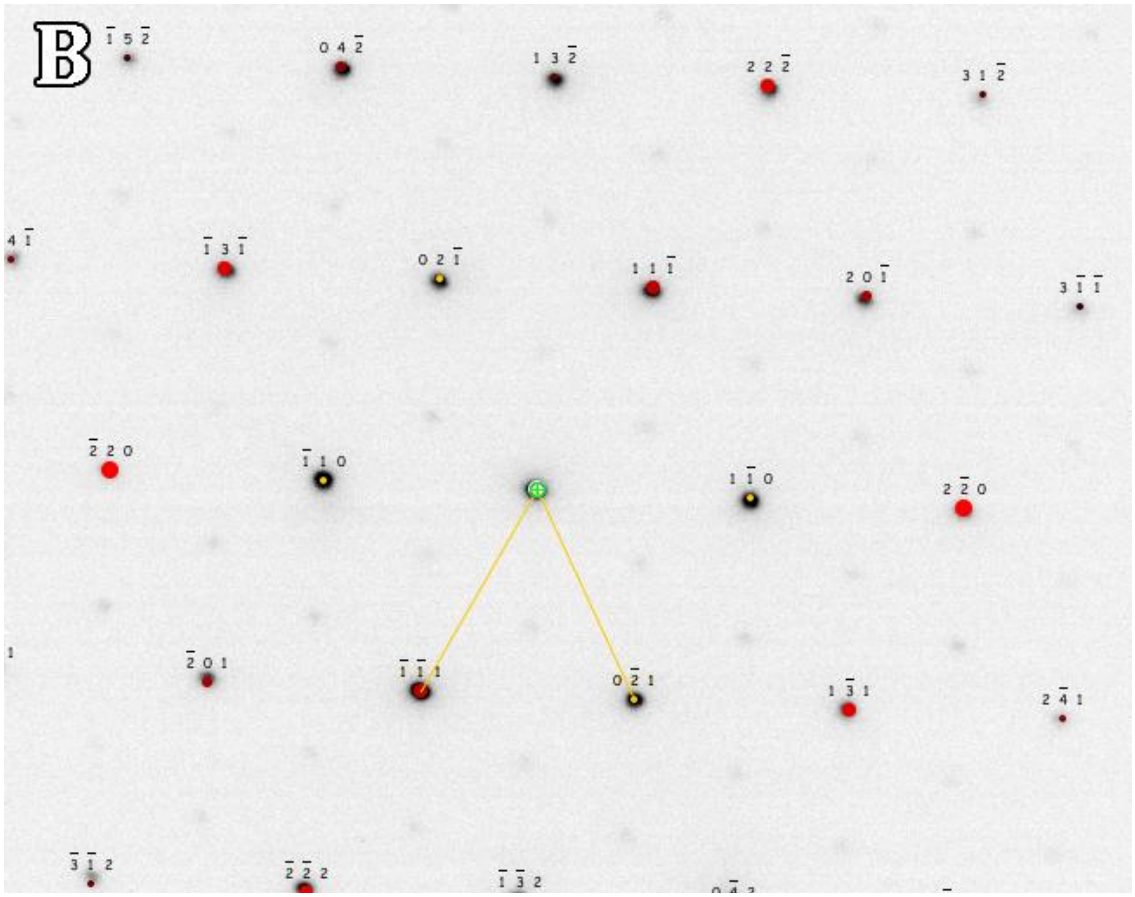

Fig. S2

Electron diffraction solutions for the (A) Kamhi and (B) Meyer orthorhombic atomic structure. The yellow spots are forbidden reflections**.**

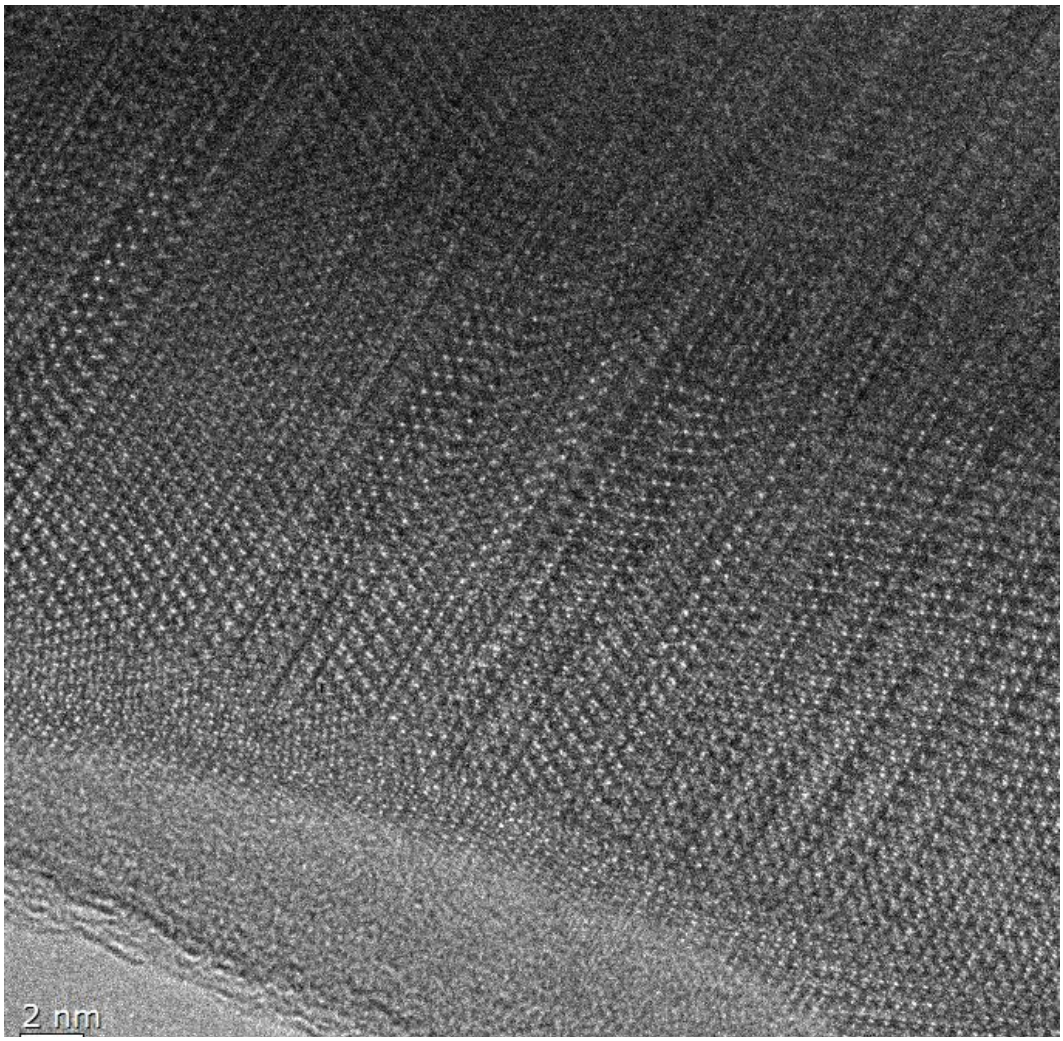

Fig. S3

HRTEM image (HV=300kV) produced from a sample cut parallel to the long axis of a single thorn, showing planar defects (stacking faults). The defects can be observed as uneven atomic spacings. Sample obtained by Ar^+ ion bombardment of different TEM sample preparations. Zone axis [210].

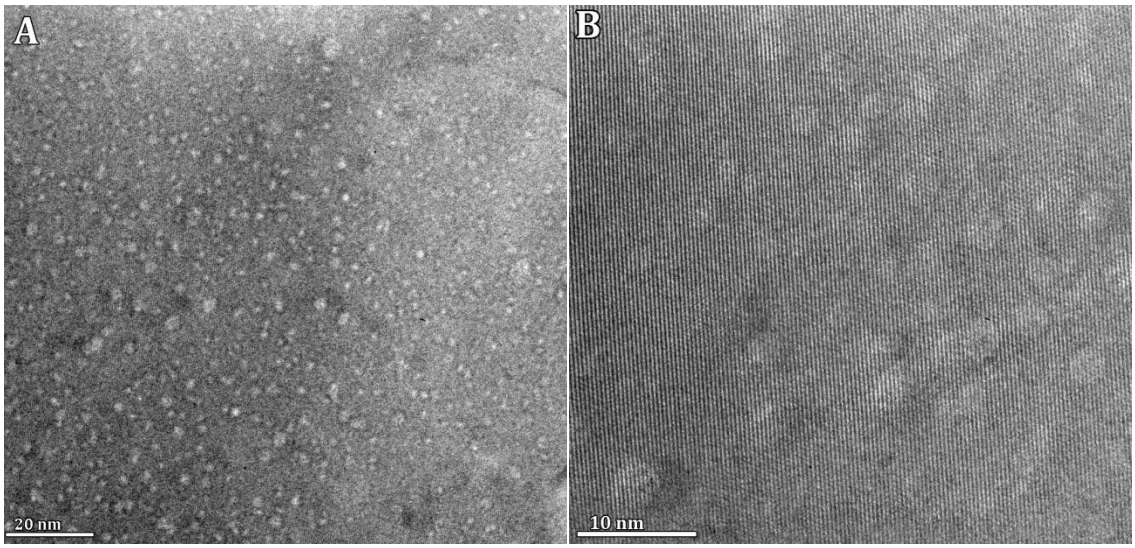

Fig. S4
TEM images (acceleration voltage 80 kV) showing both bright and darker contrast circles. A and B show bright contrast circles of the organic substance at different magnifications.

Table S1.
Fitting parameters for four of the examined models in the matching phase-contrast images presented in Fig. 2

Structure	**Fitting (0-1)**
Kamhi (hexagonal)	0.73
Meyer (orthorhombic)	0.45
Mugnaioli et al. (monoclinic)	0.29
Mugnaioli et al. (triclinic)	0.32

Table S2.

D-spaces, Å values. For calcite, aragonite and the phase contrast image see Fig. 3B

Calcite	Aragonite	Kamhi	d-spacing derived from phase contrast image fig. 3B
-	-		5.56 ± 0.01
3.86	4.66	4.25	4.72 ± 0.01
3.04	3.28	3.30	3.18 ± 0.01
-	-		2.93 ± 0.01
2.84	2.87	2.47	2.87 ± 0.01
-	2.17	2.12	2.15 ± 0.01